ACS APPLIED NANO MATERIALS

www.acsanm.org

Article

Springtail-Inspired Hierarchically Structured Polymer Films as Omniphobic Coatings for Directional Transportation of Liquids

Yu-Zhe Ye,[⊥] Shin-Hua Lin,[⊥] Shang-Yu Hsieh, Bo-Han Zeng, Han-Yu Hsueh, Chia-Feng Lin, Ya-Lien Cheng, Hsiang-Wen Hsuen, Kun-Yi Andrew Lin,* Rong-Ho Lee, and Hongta Yang*

Cite This: *ACS Appl. Nano Mater.* 2024, 7, 14584−14595

Read Online

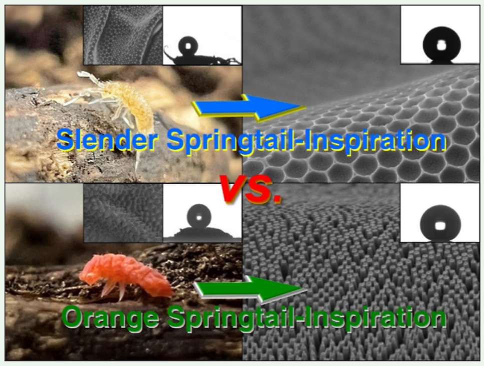

ABSTRACT: Slender springtails (*Entomobrya nivalis*) and orange springtails (*Neanura muscorum*) are capable of repelling water and organic liquids using the hexagonally arranged nanoscale waxy protrusions and microscale wrinkles on their cuticles to protect the skin-breathing arthropods against suffocation in diversified survival environments. The omniphobic hierarchical structures can even shed and directionally transport liquids along the longitudinal direction of the wrinkles. Bioinspired by springtails, monolayer colloidal crystals are self-assembled onto anisotropic microwrinkled substrates and serve as structural templates to pattern antiwetting hierarchical structure arrays. The dependence of structure configuration on the antiwetting performances is systematically investigated in this study. Impressively, the optimized structure array exhibits anisotropic omniphobic sliding characteristics toward liquids with varied surface tensions ranging from 72.8 to 27.2 mN/m. The springtail-inspired coatings undoubtedly have great potential for developing innovative applications that require directional transportation and the collection of liquids.

KEYWORDS: *springtail, omniphobic, hierarchical structures, directional transport, self-assembly*

■ INTRODUCTION

Nature is the best source of wisdom. Over billion years of natural selection, biological organisms have evolved versatile physiological architectures to realize advanced functionalities for survival under various harsh environments. To cite an instance, water-repellent scared lotus (*Nelumbo nucifera*) leaves are covered with nano/microscale waxy architectures, which considerably reduce the contact area and adhesion between water droplets and the surface.[1] The minimized interaction further leads to an increase in surface hydrophobicity and a self-cleaning property. Besides, a variety of superhydrophobic architectures are discovered on bear cicada (*Cryptotympana takasagona* Kato), water strider (*Gerridae*), lady's mantle (*Alchemilla vulgaris*), prickly pear (*Opuntia*), and nasturtium (*Tropaeolum*), to name a few.[2−6] Interestingly, reed leaves and rice leaves even exhibit anisotropic antiwetting characteristics.[7,8] The grooved hierarchical structures on their surfaces allow dew droplets to roll off along the microscale grooves for collecting water to encourage plant growth. In addition, similar dewetting architectures can also be found on animals, for example, blue morpho butterfly (*Morpho deidamia*) wings.[9,10] Bioinspired by the natural creatures, geometrically patterned surfaces have been designed and developed.[11−15] Nevertheless, their antiwetting behaviors are significantly diminished and ineffective for transportation of low-surface-tension liquids.

In sharp contrast, pitcher plant (*Nepenthes vogelii*), mignonette vine (*Anredera cordifolia*), and desert rain frog (*Breviceps macrops*) are well-known for their omniphobic surfaces, which are created by the delicate combination of grooved hierarchical structures and low-surface-energy lubricating fluids.[16−18] The lubricating fluid-infused patterns assuredly introduce a new strategy to repel the wetting of common liquids with different surface tensions and to assist or attain controllable liquid dynamics. According to the principles, slippery surfaces with anisotropic self-cleaning and omniphobic capabilities have been developed by incorporating a diversity of directional topography-based patterns and lubricants.[19−22] However, it remains a challenge to avoid the volatilization or removal of lubricant by moving liquids during the processes. The depletion of lubricants inevitably results in unstable surface properties. Therefore, there is an urgent demand to develop omniphobic coatings for the directional transportation of liquids without the use of lubricants.

Springtails, known as Collembola, are the most abundant and diverse soil-dwelling arthropods.[23,24] The arthropods primarily inhabit leaf litter niches and soil layers in the presence of water, soil microorganisms, and decaying organic/

Received: April 10, 2024
Revised: June 5, 2024
Accepted: June 10, 2024
Published: June 18, 2024

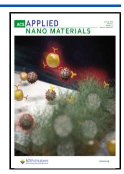

https://doi.org/10.1021/acsanm.4c02117
ACS Appl. Nano Mater. 2024, 7, 14584−14595

biological compounds. To maintain the function of cutaneous respiration, the cuticles of these microparticles are covered with hexagonally arranged nanoscale protrusions and directional microscale ridges. The hierarchical structures have been demonstrated to behave remarkable water/organic liquid-repellent properties and anisotropic self-cleaning capabilities.[25,26] Inspired by the springtails, numerous top-down fabrication methodologies are introduced to biomimic the surface morphology of springtail cuticles.[27−29] Unfortunately, most of the current photolithography-based technologies are costly, and the as-fabricated nanoscale features seriously suffer from low resolutions. Although electron beam lithography has been exploited to address the issues, the technology is still restricted by the low throughput of products and high-priced commercial masks.

On the other hand, bottom-up fabrication methodologies render an uncomplicated and low-cost alternative in constructing nanoscale structures. In the fabrication procedures, highly ordered colloidal monolayers are self-assembled and utilized as structural templates to pattern nanostructure arrays. Benefiting from the rapid progress of nanotechnologies, a wide spectrum of colloidal self-assembly approaches, including magnetic field/electric field -induced self-assembly, capillary force-induced self-assembly, evaporation-induced self-assembly, shear force-induced self-assembly, and template-assisted self-assembly, have been applied to design and build hierarchical structure arrays.[30−35] Nevertheless, most of the self-assembly approaches are time-consuming and merely favorable for laboratory-scale production. Moreover, the strategy for creating hierarchical structures, composed of hexagonally arranged nanoscale structures and directional microscale architectures, through using bottom-up fabrication technologies has rarely been reported.

In recent years, it has been evidenced that symmetric microwrinkles with precisely controllable orientations and dimensions can be achieved using a versatile interfacial release-controlled approach.[36−38] The wrinkle formation relies upon the kinetic release of local strain generated from the elastic modulus mismatch between different layers of a multilayer composite.[39,40] The wrinkle arrays can subsequently serve as templates to bring about globally aligned surface wrinkle arrays. Here, a roll-to-roll compatible modified Langmuir–Blodgett methodology is developed to further assemble silica colloidal monolayers onto polymeric wrinkle arrays. The monolayer colloidal crystals can directly function as structural templates to engineer springtail-inspired hierarchical structure arrays, which greatly reduce interactions with water or organic liquids on contact. Their static and dynamic repellencies toward common liquids on the structure arrays are investigated as well. It is believed that the as-developed omniphobic structures are capable of transporting liquids with a wide range of surface tensions directionally, which plays a vital role in human life and industrial processes, such as energy conversion systems, directional antifouling, directional drag reduction, and directional oil/water separation.[22] The resulting anisotropic wettabilities undoubtedly attract tremendous attention owing to their wide range of applications, including microfluidic devices, water collection, flow regulating devices, etc.[13−15]

■ EXPERIMENTAL SECTION

Specimens and Reagents. Slender springtail (*Entomobrya nivalis*) specimens and orange springtail (*Bilobella braunerae*) specimens are obtained from the Taiwan Muh Sheng Insect Museum and investigated without any further treatment. The chemicals applied for synthesizing Stöber silica colloids, containing absolute ethanol (≥99.8%), ammonium hydroxide (≥23.8%), and tetraethyl orthosilicate (≥99.5%), are collected from the Merck KGaA. A Milli-Q IQ 7015 ultrapure laboratory water system, which is utilized to prepare deionized water with a resistivity of 18.2 MΩ·cm at 25 °C. The deionized water is applied throughout all experiments without further purification. Ethoxylated trimethylolpropane triacrylate (ETPTA) photocurable monomers (SR 454, ≥99.5%) and 2-hydroxy-2-methyl-1-phenyl-1-propanone (HMPP) (Darocur 1173, ≥97.0%) as photoinitiators are supplied by Sartomer Americas and Merck KGaA, respectively. Poly(dimethylsiloxane) (PDMS) precursors (Sylgard 184 Silicone Elastomer Kit), containing base and curing agents, are purchased from Dow Corning. Hydrofluoric acid (HF) aqueous solution (≥48.0%) and 1*H*,1*H*,2*H*,2*H*-heptadecafluorodecyl acrylate (HDFDA) (≥97.0%) as a surface modifier are acquired from Merck KGaA. All the above chemicals are of reagent quality and are used as received. The chemicals and daily supplies used to evaluate omniphobic behaviors include glycerol (≥99.5%), ethylene glycol (≥99.5%), *n*-hexadecane (≥99.0%), ink (Colorona Mica Black), low-fat milk (1.0% milk fat), whole milk (3.8% milk fat), sunflower oil (100.0%), soybean oil (100.0%), and olive oil (100.0%), are provided by Merck KGaA and Standard Foods, respectively.

Self-Assembly of Hexagonally Arranged Nanoscale Structure Arrays. Spherical silica colloids, with average diameters of 300 and 450 nm (<3% standard deviations), are synthesized following the well-established Stöber approach.[41] The as-prepared Stöber silica colloids are cleansed in absolute ethanol through multiple dispersion/centrifugation cycles to remove any unreacted reagents and then dispersed in a mixture of ETPTA photocurable monomer and HMPP (1.5%) using a PT-MR 3100 ultrasonic homogenizer (Kinematic Polytron). After filtering the silica colloidal suspension through a 2 μm Millex syringe filter (Merck Millipore) to eliminate colloidal aggregates, the ETPTA monomer-covered silica colloids are dripped onto deionized water in a circular glass dish, where a poly(ETPTA) substrate is immersed beforehand. In this procedure, the silica colloids are assembled into a 2D hexagonal arrangement on the water surface spontaneously as a result of the surface tension difference between water and ETPTA monomers. Afterward, a DX-5A dip coater (Sadhu Design) is utilized to withdraw the poly(ETPTA) substrate upward with a constant speed of 1 mm/s, while the silica colloidal crystals are transferred onto the substrate. During the modified Langmuir–Blodgett process, the space between the silica colloids and the substrate is gradually filled by the liquiform ETPTA monomers. Subsequently, the monomers are photopolymerized in 30 s using an XLite-600F UV curing chamber (OPAS). The self-assembled silica colloidal crystals, partially embedded in the poly(ETPTA) matrix, can be selectively wet-etched by dilute HF (2.5%) to create hexagonally arranged hole arrays. Besides that, the silica colloids can serve as etching masks to pattern hexagonally arranged structure arrays in an Unaxis Shuttlelock 700 reactive ion etcher (OC Oerlikon) with a constant power density of 15 W/cm^2 and a constant chamber pressure of 20 mTorr. During colloidal lithography, argon and oxygen flow rates are varied depending on demand. After the plasma etching process, the silica etching masks are removed by dilute HF (2.5%) to develop nanoscale cylindrical and conical structure arrays.

Templating Fabrication of Microscale Wrinkles. A mixture of PDMS base/curing agent with a weight ratio of 20:1 is poured on a glass Petri dish and degassed for about half an hour in a vacuum oven (Thermo Scientific). After being cured at 75 °C for another 4 h, the solidified PDMS film is gently peeled off and shaped into cuboids (3.0 × 3.0 × 0.5 cm in width × length × height) with sharp edges. The elastomeric samples can be stretched uniaxially at a constant stretching rate of 10 cm/min on an A1-3000 electromechanical machine (GOTECH). As their elongation ratios reach 20%, the stretched samples are exposed to ultraviolet irradiation/ozone under varied treatment durations using an UVGL-25 compact UV lamp (Analytik Jena). Owing to the elastic modulus mismatch between the stiff layer and the PDMS elastomers, microscale wrinkles are spontaneously generated upon releasing the stretched film.[42,43]

Upon release, microscale wrinkles with adjustable wavelengths and amplitudes are spontaneously generated on their surfaces. Afterward, poly(ETPTA) wrinkles are replicated by conventional soft lithography.[44] A mixture of ETPTA monomer and HMPP (1.5%) is cast onto the microscale PDMS wrinkles, followed by a photopolymerization process in the UV curing chamber. On account of the low surface energy and low elastic modulus of PDMS, the as-prepared microscale wrinkled poly(ETPTA) films can be effortlessly peeled off from the PDMS molds.

Development of Springtail-Inspired Hierarchical Structure Arrays. ETPTA monomer-covered silica colloids, with average diameters of 300 and 450 nm, are subsequently self-assembled and deposited onto the microscale wrinkled poly(ETPTA) substrates through the aforenamed Langmuir−Blodgett process.[45] On account of the surface tension difference between ETPTA monomers and water, the monomer-covered silica colloids are spontaneously assembled on the water surface. After polymerization of the ETPTA monomers, the silica colloidal crystals can serve as structural templates to pattern nanoscale hole arrays, cylindrical structure arrays, or conical structure arrays onto the wrinkles in a Shutterlock-770 reactive ion etcher with an inductively coupled plasma module (Unaxis). The chamber pressure and radio frequency (RF) power are maintained at 20 mTorr and 150 W, respectively. Lastly, the silica templates are wet-etched to build springtail-inspired hierarchical structure arrays.

Surface Functionalization of Hierarchical Structure Arrays. The resulting hierarchical structure arrays can be surface-modified with fluoride to reduce their surface energies by using a chemical vapor deposition approach. For the surface functionalization process, the structure-patterned poly(ETPTA) substrates and a beaker of HDFDA are placed in a vacuum oven. Once the baking temperature reaches 75 °C under vacuum conditions, the HDFDA can be vaporized below its intrinsic boiling point and react with the acrylate groups of poly(ETPTA).[46] After 0.5 h, the chemically functionalized samples are transferred into a vacuum chamber for completely removing any unreacted HDFDA molecule.

Characterization. Photographic images of the springtail specimens are recorded directly by an XY200 compact digital camera (Canon). A JSM-7800F field-emission scanning electron microscope with energy dispersive X-ray spectroscopy (FE-SEM/EDX) (JEOL) is employed to investigate surface topographical features and quantitative elemental information on the specimens and bioinspired samples, which are sputter-coated with thin platinum layers using a Cressington 108 auto sputter coater (Ted Pella) prior to SEM imaging. Their surface morphologies are further evaluated by SPA-400 tapping-mode atomic force microscopy (Seiko Instruments) under ambient conditions. Optical microscopy images and laser scanning confocal microscopy images of microscale wrinkles are acquired from a DM4 optical microscope (Leica) and a VK-X1000 3D laser scanning confocal microscope (Keyence), respectively. Wetting behaviors, including static contact angles, advancing contact angles, receding contact liquids, and sliding angles, of all the samples are performed on a G10 drop shape analyzer system (Krüss) with an automated liquid handling system (Hamilton). Liquid drops with fixed volumes of 3 μL are pipetted onto the samples, and their images are taken 3 s after the drop applications. Afterward, DropSnake drop analysis software is utilized to shape and fit the drop profiles for determining their static and dynamic contact angles. In this research, 10 measurements of different regions of each sample are averaged and reported. The surface tensions of common liquids are evaluated using a Sigma 702 force tensiometer (Biolin Scientific).

RESULTS AND DISCUSSION

Slender Springtails. Brightly colored slender springtails (*E. nivalis*) are skin-breathing arthropods (up to 3 mm in length), which mostly inhabit overgrown grasses and the upper litter layer of fallen logs.[47,48] To protect them against suffocation by complete wetting, their entire bodies possess remarkably superhydrophobic behaviors, exhibiting both static and dynamic repellencies toward common liquids, such as raindrops. As evidenced in Figure 1a, water forms a droplet,

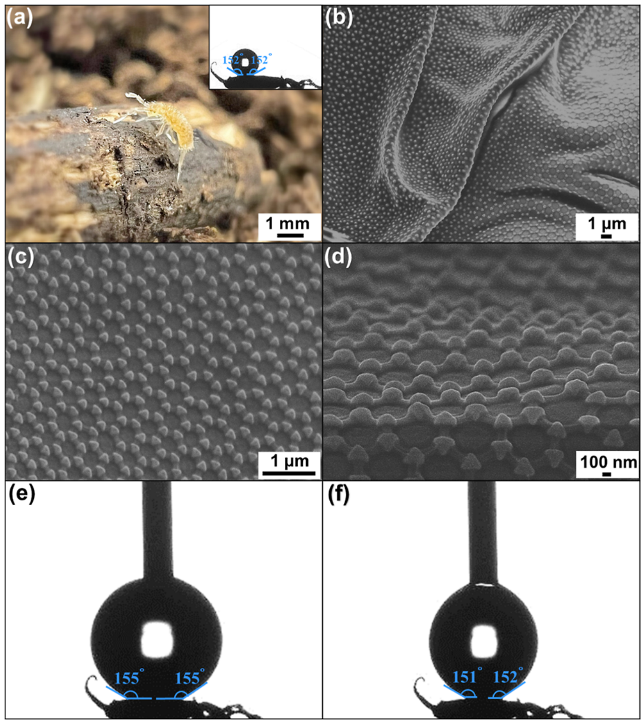

Figure 1. (a) Photographic image of a slender springtail specimen under natural sunlight illumination. Inset displaying suspension of a water droplet above the specimen. (b) Top-view SEM image, (c) magnified top-view SEM image, and (d) magnified tilted-view SEM image of the slender springtail cuticle showing hierarchical structures composed of microscale wrinkles, which are covered with hexagonally arranged nanoscale hole arrays. (e) Advancing water contact angle and (f) receding water contact angle on the specimen.

and displays a static contact angle of 152° with the underlying slender springtail. Instead of rigid and thick cuticular layers, their skins are covered with hierarchical structures composed of microscale wrinkles and nanoscale holes (Figure 1b). Astonishingly, all the holes are well-organized in a hexagonal arrangement; besides, each of them is surrounded by 6 nanoscale waxy granules (Figure 1c,d). It is worth noting that the hole size varies from 300 to 450 nm across different life stages of a slender springtail, while the wax granules are with less than 100 nm in size.[47,49] The integration of hydrophobic materials and topographic structuring substantially reduces the contact area between common liquids and their skins, making the hierarchical structures function as a low-adhesion barrier to repel and prevent the liquids from spreading out. The dynamic water contact angles during wetting/dewetting processes on the springtail are further assessed to evaluate their dynamic water-repellent properties. It is apparent that the advancing contact angle (155°) is fairly similar to the receding contact angle (151°) (Figure 1e,f); hence, it leads to a low contact angle hysteresis. The corresponding antiwetting properties allow the springtail to shed water drops and water-base debris off their skins by gravity at low sliding angles.[50]

Slender Springtail-Inspired Hierarchical Structure Arrays. Bioinspired by the antiwetting performance of slender springtails, hierarchical structure arrays are designed and built using roll-to-roll compatible colloidal self-assembly technology

https://doi.org/10.1021/acsanm.4c02117
ACS Appl. Nano Mater. 2024, 7, 14584−14595

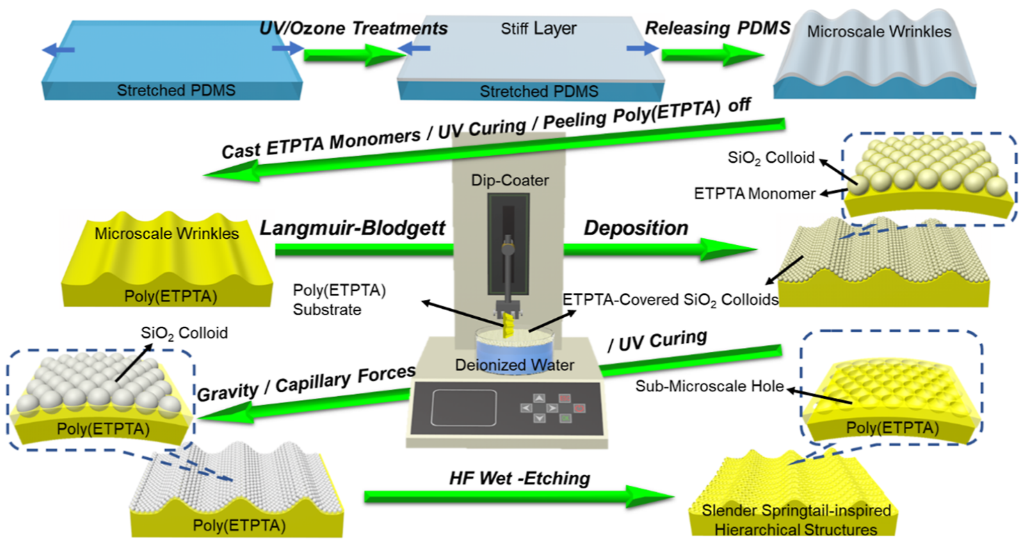

Figure 2. Schematic illustration of the steps used to engineer slender springtail-inspired hierarchical structure arrays.

(Figure 2). As mentioned previously, the springtail skins are covered with microscale wrinkles and nanoscale holes, with diameters varying from 300 to 450 nm across their life stages. To comprehend the surface morphology effect on antiwetting characteristics, hexagonally arranged 300 nm hole arrays with controllable hole opening sizes are fabricated on bare poly(ETPTA) substrates first by applying 300 nm silica colloidal suspensions with varied colloid volume fractions using the modified Langmuir−Blodgett methodology. The self-assembled monolayer silica colloidal crystals, partially embedded in poly(ETPTA) matrices, can be directly utilized as structural templates to pattern hole arrays (Figures S1 and S2). Apparently, their long-range hexagonal periodicities are well-preserved after wet-etching the silica templates. The application of colloidal suspensions with higher colloid volume fractions in the assembly process results in the formation of less polymer-embedded colloidal crystals (insets of Figures S1 and S2), and thus 300 nm hole arrays with varied opening sizes can be generated. It is worthy to mention that the bottom-hemispheres of the silica colloids are embedded in the polymeric matrix, and a maximum hole opening size (300 ± 5 nm) is therefore achieved as the colloid volume fraction reaches 35 vol % (Figure S3). Each of the resulting hemispherical holes is surrounded by 6 nanoscale sharp protuberances, which prevent liquids that bridge them from contacting the nanoscale holes after a chemical functionalization with fluoride to reduce their surface energies from 59.0 to 7.7 mN/m (Figure S4). As a result, the introduction of hemispherical holes can effectively enhance the antiwetting capabilities (Figures S5 and S6). It is evident that a maximum static water contact angle of 154 ± 1° and a minimum water contact angle hysteresis of 8° are achieved on the surface-modified hemispherical hole array. The contact angle hysteresis refers to the difference between advancing and receding contact angles (159 ± 1°/150 ± 1°). On the other hand, the usage of colloidal suspensions with even higher colloid volume fractions brings about much less polymer-embedded silica colloids and hence develops hole arrays with smaller openings. The increased solid projected area fractions inevitably hinder their corresponding antiwetting performances. The results can be described theoretically using the Cassie−Baxter dewetting equation

$$\cos\theta_c = f\cos\theta - (1 - f)$$

where θ_c and θ represent the static water contact angle and the intrinsic water contact angle (107 ± 1°) (Figure S5), respectively. Besides, f denotes the solid projected area fraction, which can be expressed by the following equation

$$f = 1 - \left(\frac{\pi R_o^2}{2\sqrt{3}\,R_s^2}\right)$$

where R_o and R_s are radii of the hole openings and the templating 300 nm silica colloids, respectively. Accordingly, the f, estimated through inserting the measured R_o (Figure S2) in this equation, can be applied in the Cassie−Baxter dewetting equation to collect θ_c. It is found that the solid projected area fraction (f) decreases with the increase of silica colloid volume fraction and attains a minimum value as the volume fraction reaches 35 vol %, whereas the calculated static water contact angle achieves a maximum angle (Figure S7). Clearly, the calculated results follow a tendency similar to that of the experimental data under varied colloid volume fractions, further suggesting that their surface hydrophobicities are predictable and controllable. Toward a better comprehension of the structure size effect on antiwetting behaviors, hexagonally arranged 450 nm hole arrays with varied hole opening sizes are templated by Langmuir−Blodgett-assembled 450 nm silica colloidal crystals (Figures S8 and S9). Identically, the application of 450 nm hemispherical holes bring about a maximum static water contact angle of 155 ± 1° and a minimum water contact angle hysteresis of 8° (Figures S10 and S11) as the colloid volume fraction reaches 35 vol %. In comparison with the static and dynamic water contact angles of 300 nm hemispherical hole arrays, it is evident that the static and dynamic repellencies toward water are only slightly enhanced through introducing 450 nm hemispherical holes.

To biomimic the hierarchical structures of slender springtails, the hexagonally arranged 450 nm hemispherical holes are subsequently assembled onto microscale wrinkles for further reduction of the solid projected area fraction. In this research, regularly orientated PDMS wrinkle arrays with adjustable wavelengths and amplitudes are utilized as templates to pattern various wrinkled poly(ETPTA) substrates. The PDMS wrinkle arrays are formed upon the release of uniaxially stretched

https://doi.org/10.1021/acsanm.4c02117
ACS Appl. Nano Mater. 2024, 7, 14584−14595

PDMS substrates, which have been treated by UV/ozone exposure for varied durations to build stiff surfaces on the elongated substrates. Apparently, microscale wrinkles are not created on the surface under a limited UV/ozone treatment (10 min) since the whole substrate still possesses consistent elastomeric properties (Figure S12a,b). By contrast, microscale wrinkle arrays perpendicular to the elongation direction are established on the long-term UV/ozone-treated PDMS substrates (Figure S12c−j). Under longer UV/ozone treatments, the increased elastic modulus mismatches lead to the formation of microscale wrinkles with larger wavelengths and amplitudes (Figure S13).[47] Afterward, microscale poly(ETPTA) wrinkles with varied wavelengths and amplitudes are replicated from the wrinkled PDMS molds by a standard soft lithography approach (Figure S14). The presence of microscale structures does not greatly reduce the solid projected area fraction. As evidenced, a maximum static water contact angle of 123 ± 2° can be achieved in the direction parallel to the surface-modified poly(ETPTA) wrinkles, replicated from a 40 min-UV/ozone-treated wrinkled PDMS mold (Figures S15−S17). Interestingly, the microscale wrinkle array displays an anisotropic antiwetting characteristic. Its corresponding water contact angle hysteresis (21°) in the direction parallel to the wrinkles is much smaller than that (35°) in the direction perpendicular to the structures. The findings disclose that liquids on these wrinkled structures tend to move along the longitudinal direction of the patterns.[51]

The microscale patterns are further integrated with nanoscale holes to enhance their geometrically antiwetting characteristics. Herein, Langmuir−Blodgett-assembled monolayer 450 nm silica colloidal crystals are directly deposited onto the microscale wrinkles, regardless of the wavelength and amplitude, for designing and building hemispherical holes (Figures S18, S19, 3, and S20). Crucially, cracks do not appear in the SEM images, indicating that the wrinkles are fully covered by the silica colloidal crystals. After the silica templates are eliminated, the long-range hexagonally arranged 450 nm hemispherical hole array-covered poly(ETPTA) wrinkle arrays are further surface-modified to reduce their surface energies. To systematically evaluate their water-repellent behaviors, static water contact angles, advancing water contact angles, receding water contact angles, and sliding angles on the resulting hierarchical structure arrays are assessed (Figures S21−S24). Their corresponding solid projected area fractions can also be estimated using the experimental data displayed previously (Figures S11 and S17). It is evident that the 450 nm hemispherical hole array-covered microscale wrinkle array, replicated from a 40 min UV/ozone-treated wrinkled PDMS mold, has the smallest solid projected area fraction (Figure 4a). On that, the specimen exhibits a maximum static water contact angle of 163 ± 2° and a minimum water contact angle hysteresis of 4° in the direction parallel to the wrinkles (Figure 4b). It is worthy to mention that the antiwetting performance is even more competitive with that of a slender springtail (Figure 1). Importantly, in comparison with the surface topographical features of nanoscale hole arrays or microscale wrinkle arrays, the slender springtail-inspired hierarchical structure arrays undoubtedly possess much smaller solid projected area fractions (Figure 4c) and hence result in the reinforcement of static and dynamic repellencies toward water (Figure 4d,e). More importantly, the presence of an oriented wrinkle array provides an asymmetric retention force that facilitates the transportation of water drops along the longitudinal direction of the wrinkles and the pinning of water drops in the opposite direction (Figure S25).[52] Even though the water contact angle hystereses are significantly decreased in both directions, their anisotropically antiwetting features are well-retained. A minimum sliding angle of 4 ± 1° can be achieved in the direction parallel to the hemispherical hole array-covered wrinkles, while the sliding angle reaches 10 ± 1° in the direction perpendicular to these wrinkles (Figure 4f). The results reveal that water drops are capable of rolling off and taking contaminants away more easily along the longitudinal direction of the wrinkles. In spite of that, the self-cleaning properties are considerably diminished toward liquids with lower surface tensions.

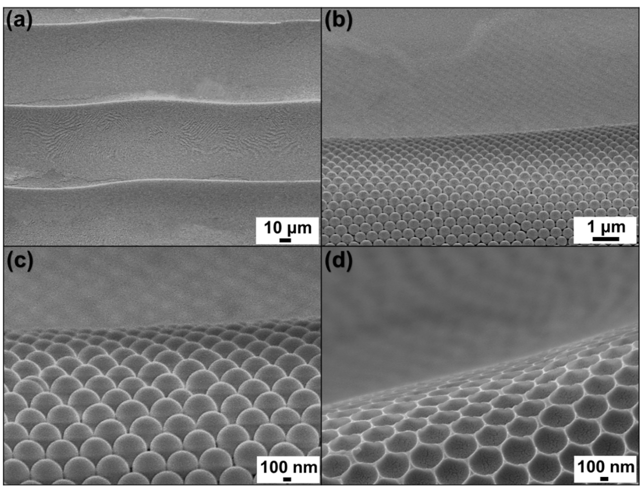

Figure 3. (a) Top-view SEM image, (b) magnified top-view SEM image, and (c) magnified tilted -view SEM image of 450 nm silica colloidal crystal-coated poly(ETPTA) wrinkles. Wrinkles are replicated from a wrinkled PDMS mold, which is fabricated under 40 min of UV/ozone treatment. (d) Magnified tilted-view SEM image of the corresponding 450 nm hole array-covered poly(ETPTA) wrinkles.

Orange Springtails. By contrast, orange springtails (*Neanura muscorum*), largely inhibiting rotten woods and mineral soil layers, can even prevent their whole bodies from wetting by low-surface-tension organic liquids or biological species (Figure 5a).[53,54] The impressive omniphobic behaviors are attributed to the presence of much more complex hierarchical structures on their cuticles. It is evidenced that the cuticles are covered with interconnected corn-shaped ridges, while each of the corn kernel-like structures is composed of a microscale protuberance and hexagonally arranged nanoscale holes (Figure 5b−d). The holes, with diameters ranging from 300 to 450 nm, are surrounded by nanoscale waxy granules. In comparison with the hole array-covered wrinkles found on the slender springtail cuticles, these protuberance-covered wrinkles assuredly allow more air to be trapped among the structures and thus possess an even higher surface hydrophobicity. As presented in Figure 5a,e,f, a large static water contact angle of 161 ± 2° and a low water contact angle hysteresis of less than 3° can be obtained on the orange springtail specimen. Bioinspired by the orange springtails, their complicated hierarchical structures are engineered following the aforementioned methodology (Figure S26). In the fabrication procedures, Langmuir−Blodgett-assembled monolayer silica colloidal crystals are deposited onto wrinkled

https://doi.org/10.1021/acsanm.4c02117
ACS Appl. Nano Mater. 2024, 7, 14584−14595

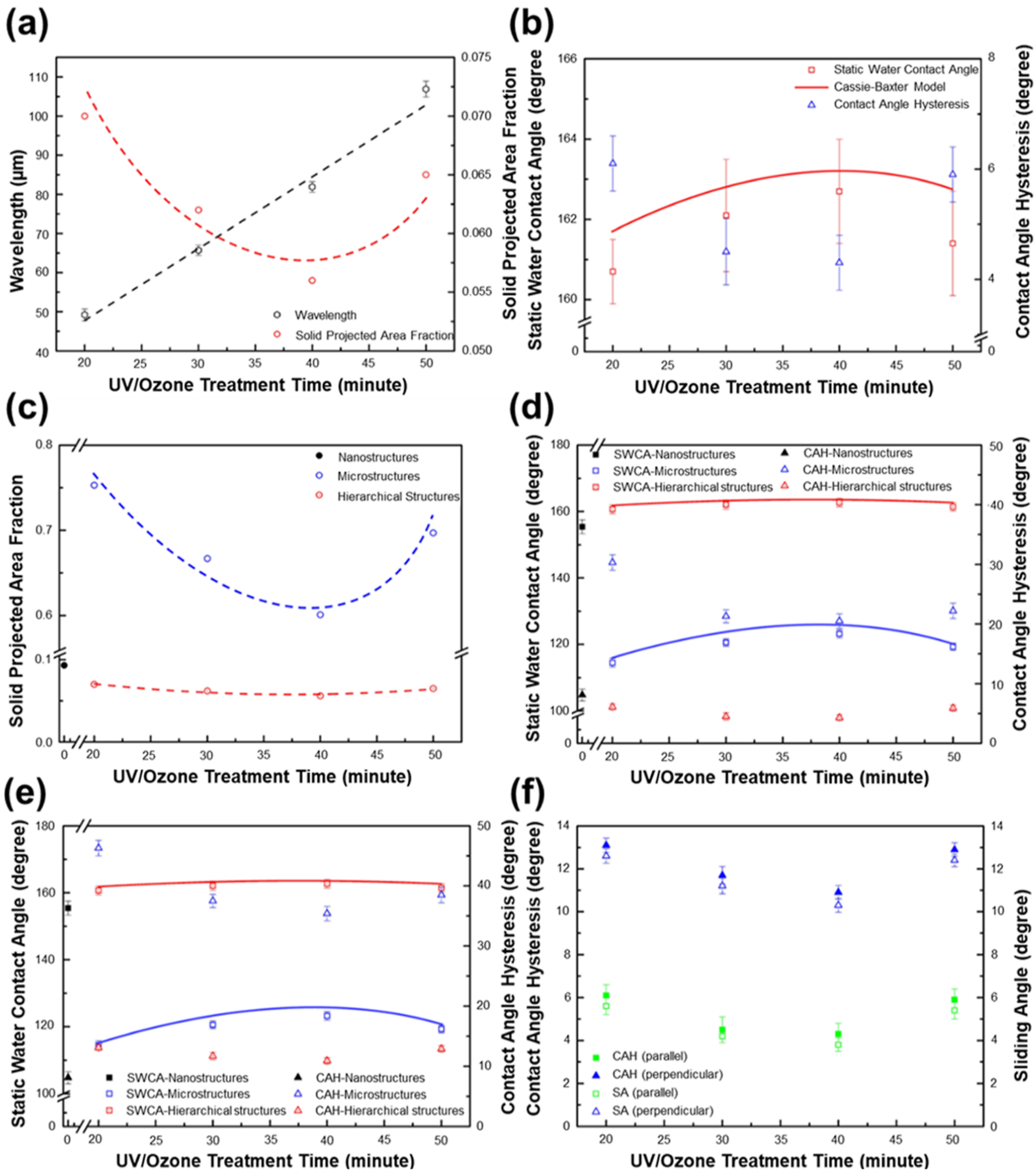

Figure 4. (a) Dependence of the wavelength (black hollow circle) on the solid projected area fraction (red hollow circle) of the surface-modified 450 nm hole array-covered poly(ETPTA) wrinkles. Structures are replicated from distinct wrinkled PDMS molds, which are fabricated under varied UV/ozone treatment durations. (b) Static water contact angles (red hollow square) and contact angle hystereses (blue hollow triangle) on the samples. (c) Comparison of the solid projected area fractions of the 450 nm hole array (black solid circle), the poly(ETPTA) wrinkles (blue hollow circle), and the 450 nm hole array-covered poly(ETPTA) wrinkles (red hollow circle). (d) Static water contact angles (square) and contact angle hystereses (triangle) on the samples. The water droplet profiles, taken in the direction perpendicular to the poly(ETPTA) wrinkles, showing the wetting behaviors and self-cleaning properties in the direction parallel to the wrinkles. (e) Static water contact angles (square) and contact angle hystereses (triangle) on the samples. The water droplet profiles, taken in the direction parallel to the poly(ETPTA) wrinkles, showing the wetting behaviors and self-cleaning properties in the direction perpendicular to the wrinkles. (f) Contact angle hystereses and sliding angles of the surface-modified 450 nm hole array-covered poly(ETPTA) wrinkles in both directions.

substrates and serve as structural templates to construct hole-patterned protuberance-covered wrinkle arrays.

Orange Springtail-Inspired Hierarchical Structure Arrays. To identify the optimal design of antiwetting structures, nanoscale hole-patterned protuberances with varied heights, shapes, and sizes are developed. First of all, a monolayer of hexagonally ordered 300 nm silica colloidal crystals is assembled and transferred on a featureless poly(ETPTA) substrate by the modified Langmuir−Blodgett technology (Figure S27a,b). The as-prepared silica colloidal-

https://doi.org/10.1021/acsanm.4c02117
ACS Appl. Nano Mater. 2024, 7, 14584−14595

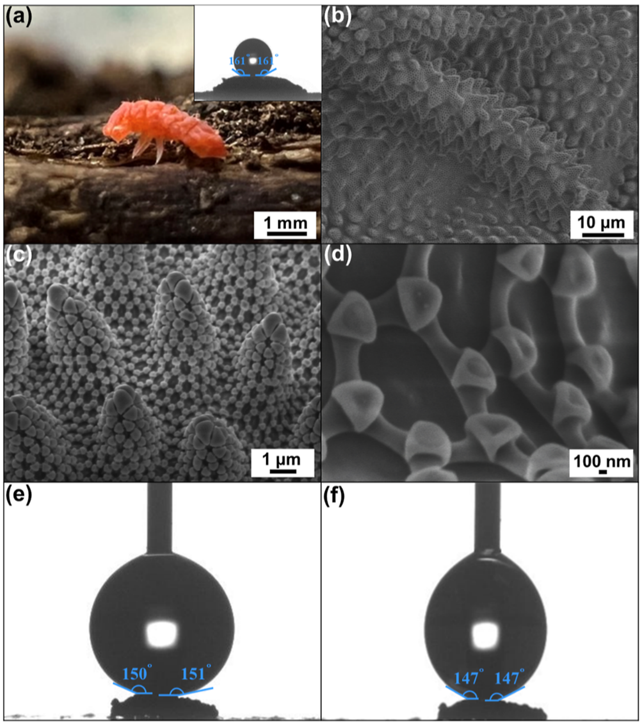

Figure 5. (a) Photographic image of an orange springtail specimen under natural sunlight illumination. Inset displaying suspension of a water droplet above the specimen. (b) Top-view SEM image, (c) magnified top-view SEM image, and (d) magnified tilted-view SEM image of the orange springtail cuticle showing hierarchical structures composed of microscale wrinkles and protuberances, which are covered with hexagonally arranged nanoscale hole arrays. (e) Advancing water contact angle and (f) receding water contact angle on the specimen.

crystal-coated substrate is then plasma etched by anisotropic argon reactive ions (40 sccm) under different plasma etching durations. In the etching process, the silica colloids are utilized as etching masks to shield the polymer underneath, leading to the formation of kokeshi-doll-like features (Figure S27c–h). After the spherical silica tops are wet-etched, long-range hexagonally arranged pillar-shaped structures, with varied heights of 150, 300, and 450 nm, are generated. Clearly, the application of longer plasma etching duration results in the configuration of higher pillar-shaped structures; besides, the cylindrical structure diameter can be determined by the silica colloid size. It is worth mentioning that the holes templated from the silica colloids are well-retained, although they are shirked slightly in the plasma etching process. Furthermore, truncated cone-shaped structures, with varied heights of 150, 300, and 450 nm, are engineered through the combination of argon reactive ion etching (30 sccm) and oxygen reactive ion etching (10 sccm) for 3, 4, and 5 min, respectively (Figure S28). Owing to the presence of isotropic oxygen reactive ion etching, the upper truncated cone-shaped features become even narrower with the increase of etching duration, and thus, they bring about a nonclose-packed appearance and a smaller solid projected area fraction. Accordingly, their static water contact angles gradually increase with the structural heights and reach a maximum value of 158 ± 1° on the surface-modified 450 nm-tall truncated cone-shaped structure array (Figure S29). As anticipated, the corresponding water contact angle hystereses decrease with the increase of structural height, while a minimum water contact angle hysteresis of 8° can be achieved. In comparison, the static water contact angles (151 ± 1°) and water contact angle hysteresis (12°) almost remain unchanged on the surface-modified pillar-shaped structures, regardless of their structural heights. To gain a better understanding of the structure effect, hexagonally arranged 450 nm-tall pillar-shaped structures and 450 nm-tall truncated cone-shaped structures are templated from monolayer 450 nm silica colloidal crystals under varied reactive ion etching conditions (Figure S30). After a surface modification treatment, the pillar-shaped structure array has a static water contact angle of 155 ± 1° and a water contact angle hysteresis of 11°, while a static water contact angle of 158 ± 1° and a water contact angle hysteresis of 6° are achieved on the truncated cone-shaped structure array (Figure S31). Interestingly, their antiwetting performances are even superior to those of the 450 nm-tall structure arrays templated from 300 nm silica colloidal crystals (Figure S32). The results can then be expounded by the Cassie–Baxter equation, where the solid projected area fractions (*f*s) are estimated using magnified top-view SEM images of the as-fabricated structure arrays (Figure S33). By assuming that the ring-shaped regions of the structures in contact with a water drop are with a mean width of 20 nm, it is found that the truncated cone-shaped structures templated from 450 nm silica colloids possess a minimum f of 0.10 and a maximum static water contact angle of 158°. Evidently, the calculated value agrees well with the experimental one, further indicating that the dewetting model can be applied to theoretically predict and adjust the geometrically antiwetting characteristics.

The aforementioned 450 nm-tall structure arrays are subsequently engineered onto the microscale wrinkle array, replicated from a 40 min-UV/ozone-treated wrinkled PDMS mold, to biomimic the hierarchical structures of soil-dwelling orange springtails. Although a few defects are presented, it is apparent that the microscale wrinkles are fully covered by nanoscale hole-patterned structure arrays (Figures 6 and 7). In addition, their long-range hexagonal arrangements are well-preserved. It is of great importance to mention that the integration of nanoscale structures and microscale wrinkles provides an elegant design to minimize the interaction with water drops. Toward a better comprehension, their *f*s are estimated using the data disclosed in Figures S17 and S33. It is evidenced that the smallest f of 0.06 is generated through introducing the 450 nm-tall truncated cone-shaped structure array, which is templated from monolayer 450 nm silica colloidal crystals (Figure 8a). As a consequence, the resulting hierarchical structure array can achieve a maximum static water contact angle of 170 ± 1° and a minimum water contact angle hysteresis of 3° in the direction parallel to the wrinkles (Figure S34), which are competitive with the antiwetting performance found on an orange springtail. In comparison, the water contact angle hysteresis reaches 9° in the direction perpendicular to the wrinkles (Figure S35). The contact angle hysteresis difference doubtlessly implies that the orange springtail-inspired hierarchical structure array allows liquids on contact to be transported directionally (Figure S36).

Besides water (γ = 72.8 mN/m), various chemicals and daily supplies, including glycerol (γ = 64.0 mN/m), low-fat milk (γ = 50.4 mN/m), whole milk (γ = 50.2 mN/m), ethylene glycol (γ = 48.4 mN/m), ink (γ = 40.5 mN/m), sunflower oil (γ = 31.4 mN/m), soybean oil (γ = 31.2 mN/m), olive oil (γ = 30.8 mN/m), and *n*-hexadecane (γ = 27.2 mN/m), are applied to

https://doi.org/10.1021/acsanm.4c02117
ACS Appl. Nano Mater. 2024, 7, 14584–14595

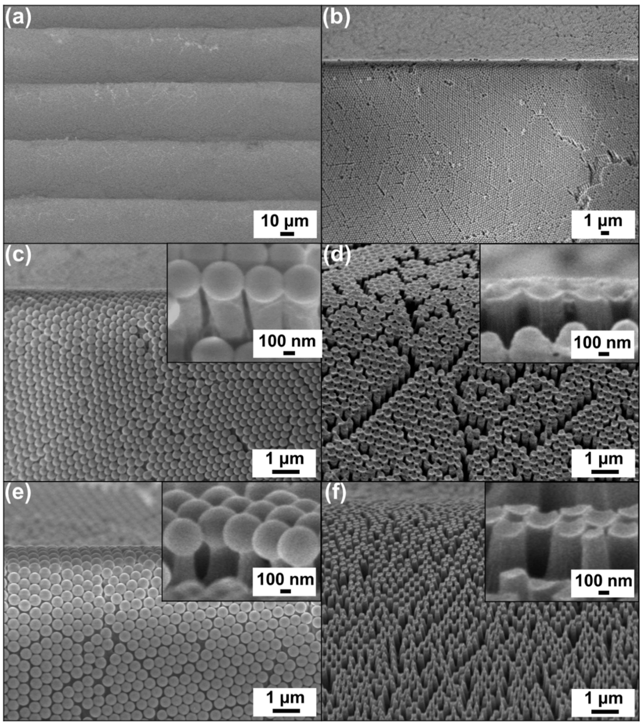

Figure 6. (a) Top-view SEM image of monolayer 300 nm silica colloidal crystals on a wrinkled poly(ETPTA) substrate. (b) Magnified SEM image of (a). Tilted-view SEM images of the hexagonally arranged kokeshi-doll-like structure arrays and their corresponding structure arrays templated from monolayer 300 nm silica colloidal crystals on the wrinkled substrate under varied reactive ion etching conditions for 5 min. (c), (d) Ar (40 sccm) and (e), (f) Ar (30 sccm)/O_2 (10 sccm). Inserts displaying magnified cross-sectional SEM images.

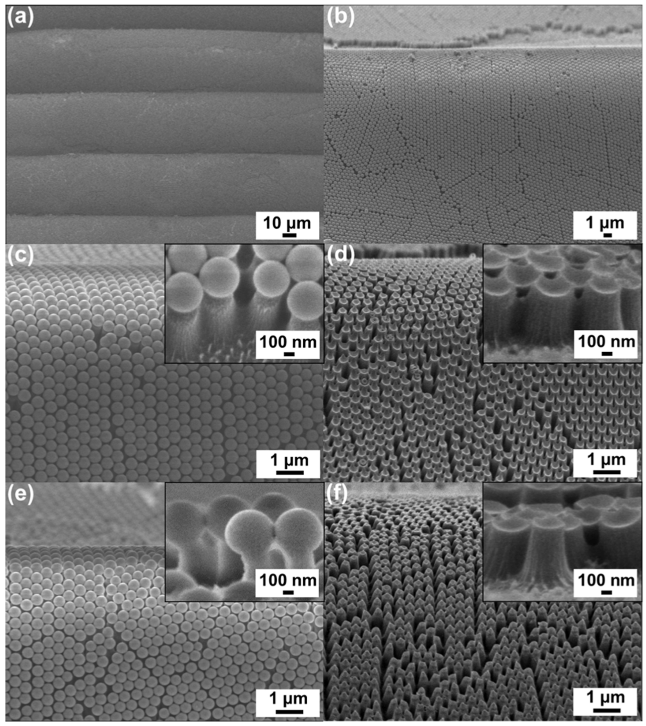

Figure 7. (a) Top-view SEM image of monolayer 450 nm silica colloidal crystals on a wrinkled poly(ETPTA) substrate. (b) Magnified SEM image of (a). Tilted-view SEM images of the hexagonally arranged kokeshi-doll-like structure arrays and their corresponding structure arrays templated from monolayer 450 nm silica colloidal crystals on the wrinkled substrate under varied reactive ion etching conditions for 5 min. (c), (d) Ar (40 sccm) and (e), (f) Ar (30 sccm)/O_2 (10 sccm). Inserts displaying magnified cross-sectional SEM images.

evaluate the corresponding static and dynamic repellencies toward common liquids with different surface tensions (Figures S37–S39). As summarized in Figure 8b, static contact angles of 161 ± 3° (glycerol), 152 ± 1° (low-fat milk), 150 ± 1° (whole milk), 145 ± 2° (ethylene glycol), 130 ± 1° (ink), 111 ± 2° (sunflower oil), 110 ± 2° (soybean oil), 103 ± 2° (olive oil), and 93 ± 2° (*n*-hexadecane), are realized on the nanoscale hole-patterned truncated cone-shaped structure-covered microscale wrinkle array. Obviously, these static contact angles are much larger than the ones found on the surface-modified 450 nm silica colloidal crystal-covered poly(ETPTA) wrinkled substrate (Figure S40). In spite of that, the static repellency toward low-surface-tension liquids is gradually decreased with the decrease of surface tension. Benefiting from the highly ordered arrangement of hierarchical structures, the antiwetting behaviors can also be assessed using the Cassie–Baxter model. In the case of f equals to 0.06, the dependence of static contact angle on surface tension can be theoretically plotted as the red solid curve. Unexpectedly, only the static contact angles of water and glycerol are located on the curve. The results are induced by the fact that low-surface-tension liquids are able to infiltrate the nanoscale structures and thus bring about an increase in f. As their surface tensions range from 50.4 to 40.5 mN/m, the nanoscale holes can be completely filled with the liquids, which leads to an abrupt increase in f (0.23, Figure S33). Accordingly, the static contact angles of low-fat milk, whole milk, ethylene glycol, and ink are located on the red dashed curve. For the liquids with even lower surface tensions (~30 mN/m), they can penetrate through the nanoscale structure array to reach the upper part of the microscale wrinkle array. Consequently, the static contact angles of cooking oils and *n*-hexadecane are greatly decreased and located on the red dotted curve (f = 0.59, Figure S17). In spite of that, all the abovementioned static contact angles are larger than 90°, which confirms its omniphobic behaviors. Although the contact angle hysteresis and sliding angles are increased with the decrease of surface tension (Figure 8c,d), its anisotropically dynamic repellency toward low-surface-tension liquids is evidenced as well. Crucially, low-surface-tension liquid droplets, such as ethylene glycol droplets, can easily roll-off the surface-modified orange springtail-inspired hierarchical structure array in less than 1 s (Figure S41). After that, the corresponding static contact angle, advancing contact angle, and receding contact angle even remained unchanged (Figure S42). The findings verify its remarkable self-cleaning performance for liquid contaminates.

To better comprehend the omniphobic behaviors of the springtail-inspired hierarchical structure arrays, static contact angles and sliding angles of various liquids on the surface-modified 450 nm hole array-covered poly(ETPTA) wrinkled substrate are evaluated as well (Figure S43). In comparison, these static contact angles are decreased from 163 ± 2 to 71 ± 2° as the surface tension of liquid varies from 72.8 to 27.2 mN/m, while the corresponding sliding angles are increased significantly with the decrease of surface tension. As evidenced, the contact angles of olive oil and *n*-hexadecane are even

https://doi.org/10.1021/acsanm.4c02117
ACS Appl. Nano Mater. 2024, 7, 14584−14595

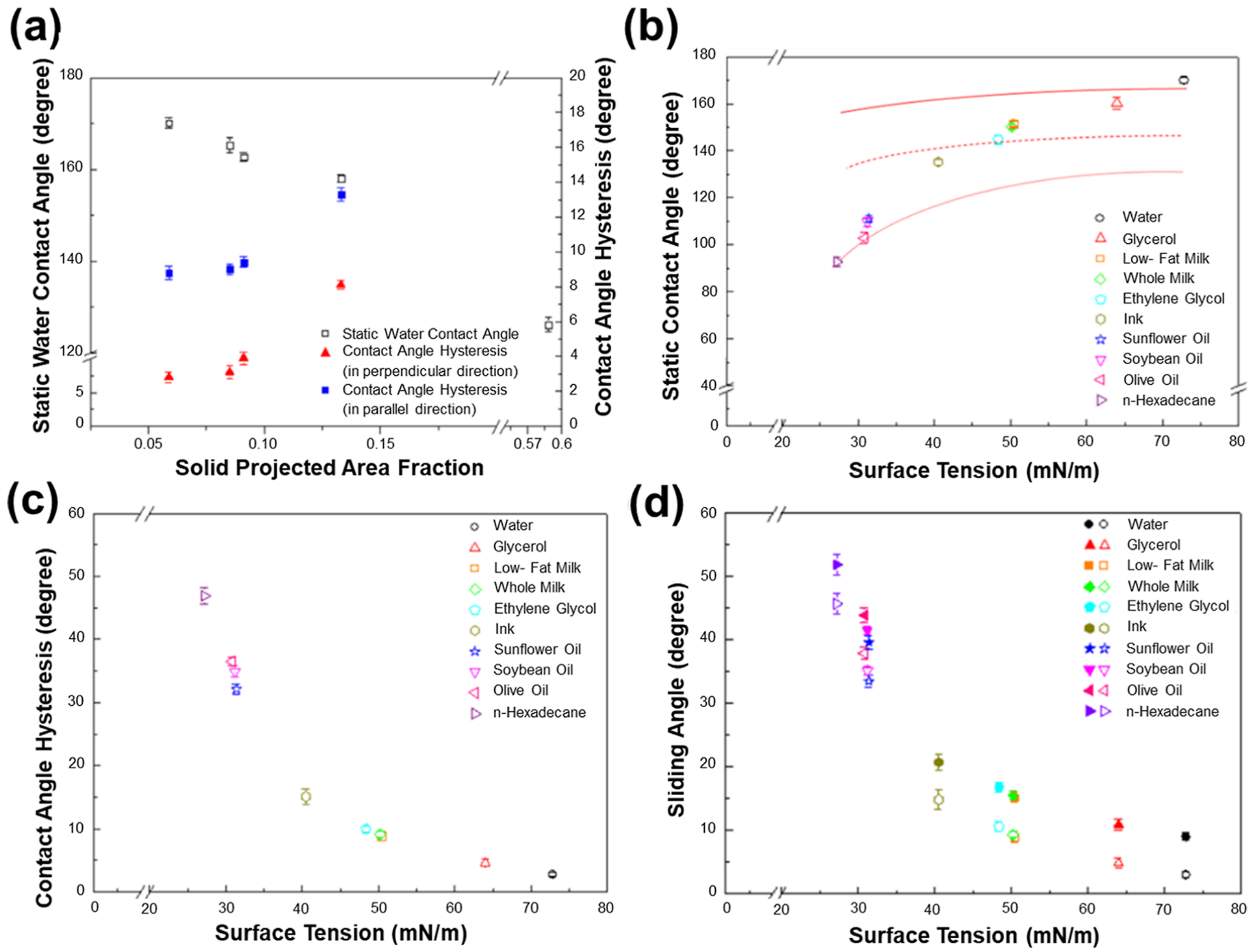

Figure 8. (a) Static water contact angles (black hollow square) and contact angle hystereses (red solid triangle/blue solid square) of the surface-modified hierarchical structure arrays templated from monolayer silica colloidal crystals on poly(ETPTA) wrinkled substrates. (b) Static contact angles and (c) contact angle hystereses of various liquids on the surface-modified hierarchical truncated cone-shaped structure array templated from monolayer 450 nm silica colloidal crystals on a poly(ETPTA) wrinkled substrate showing the wetting behaviors in the direction parallel to the wrinkles. (d) Sliding angles of various liquids on the sample showing the self-cleaning properties in the direction parallel to (hollow symbols)/perpendicular to (solid symbols) the wrinkles.

smaller than 90°. The findings further disclose that the antiwetting characteristics on the slander springtail-inspired geometry are greatly impaired by low-surface-tension liquids. It is believed that the orange springtail-inspired hierarchal structure array allows more air to be trapped between the structures and possesses much smaller interactions with liquid drops of varied surface tensions. As a result, the orange springtail-inspired geometry brings about enhanced static and dynamic repellencies toward common liquids. To further demonstrate their self-cleaning abilities for solid contaminants, chalk powders are deliberately sprinkled onto both of the surface-modified springtail-inspired hierarchical structure array-covered substrates (Figure S44). It is observed that the chalk powders can be picked up by rolling water droplets, leaving clear paths behind. Importantly, more powders are removed from the orange springtail-inspired hierarchical structure array-covered substrate, resulting in a cleansed appearance.

The capacity of a particular coating to withstand superficial mechanical forces is another critical issue to investigate in terms of its environmental durability. Here, a constant-load scratch test according to the ASTM D3363 method is applied to determine the mechanical properties of as-fabricated springtail-inspired hierarchical structure array-covered substrates using a pencil set with varied hardness grades ranging from 1H to 6H.[55] In the experimental process, the selected pencil with a load of 10 N is placed on the coating and forms a 45° angle with the surface. The highest pencil grade that is unable to cause damage after 500 rubbing cycles is considered as the corresponding mechanical properties. As displayed in Figure S45, their static water contact angles and water contact angle hysteresis are well-maintained after a 4H pencil hardness test. On the contrast, its intrinsic antiwetting behaviors are impaired after scratching with a 5 H pencil. The mechanical properties are even more competitive with commercial coatings.[56]

■ CONCLUSIONS

In conclusion, monolayer close-packed silica colloidal crystals are self-assembled onto microscale wrinkle arrays to serve as structural templates for engineering omniphobic hierarchical structure arrays, which are inspired by slender springtails and orange springtails. Importantly, the size, shape, and height of the hierarchical structures can be controlled through applying varied-sized silica colloids with different colloid volume fractions or adjusting the plasma etching parameters. It is evident that the slender springtail-inspired hole-covered wrinkle array exhibits superhydrophobic and self-cleaning characteristics. In comparison with that, the static and dynamic repellencies toward common liquids are significantly enhanced on the orange-spring-tail-inspired hierarchical structure array. The integration of nanoscale hole-patterned truncated cone-shaped structure arrays and microscale wrinkle arrays demonstrates an elegant design to minimize interaction with liquid drops of varied surface tensions and subsequently endows the drop motion with directionality. It appears that the springtail-inspired antiwetting structure arrays will ultimately contribute to practical fluid-controlling tasks such as liquid harvesting, microfluidic devices, biomedical applications, and beyond.

■ ASSOCIATED CONTENT

Supporting Information

The Supporting Information is available free of charge at https://pubs.acs.org/doi/10.1021/acsanm.4c02117.

> Surface morphologies of monolayer silica colloidal crystals, hole arrays, wrinkle arrays, colloidal crystal-covered wrinkle arrays, slander springtail-inspired hierarchical structure arrays, pillar-shaped structure arrays; static contact angles, advancing contact angles, receding contact angles, and sliding angles on the surface-modified featureless poly(ETPTA) substrate, hole arrays, wrinkle arrays, slander springtail-inspired hierarchical structure arrays, pillar-shaped structure arrays, orange springtail-inspired hierarchical structure arrays, colloidal crystal-covered wrinkle arrays; and schematic illustration of the steps used to engineer the springtail-inspired hierarchical structure array and the corresponding anisotropically antiwetting mechanisms (PDF)

■ AUTHOR INFORMATION

Corresponding Authors

Kun-Yi Andrew Lin − *Department of Environmental Engineering, National Chung Hsing University, Taichung 40227, Taiwan; Institute of Analytical and Environmental Sciences, National Tsing Hua University, Hsinchu 300044, Taiwan;* orcid.org/0000-0003-1058-3097; Email: linky@nchu.edu.tw

Hongta Yang − *Department of Chemical Engineering, National Chung Hsing University, Taichung 40227, Taiwan;* orcid.org/0000-0002-5822-1469; Email: hyang@dragon.nchu.edu.tw

Authors

Yu-Zhe Ye − *Department of Chemical Engineering, National Chung Hsing University, Taichung 40227, Taiwan*

Shin-Hua Lin − *Department of Chemical Engineering, National Chung Hsing University, Taichung 40227, Taiwan*

Shang-Yu Hsieh − *Department of Chemical Engineering, National Chung Hsing University, Taichung 40227, Taiwan*

Bo-Han Zeng − *Department of Chemical Engineering, National Chung Hsing University, Taichung 40227, Taiwan*

Han-Yu Hsueh − *Department of Materials Science & Engineering, National Chung Hsing University, Taichung 40227, Taiwan;* orcid.org/0000-0003-2850-7279

Chia-Feng Lin − *Department of Materials Science & Engineering, National Chung Hsing University, Taichung 40227, Taiwan;* orcid.org/0000-0002-1743-4337

Ya-Lien Cheng − *Department of Chemical Engineering, National Chung Hsing University, Taichung 40227, Taiwan*

Hsiang-Wen Hsuen − *Department of Chemical Engineering, National Chung Hsing University, Taichung 40227, Taiwan*

Rong-Ho Lee − *Department of Chemical Engineering, National Chung Hsing University, Taichung 40227, Taiwan*

Complete contact information is available at: https://pubs.acs.org/10.1021/acsanm.4c02117

Author Contributions

⊥Y.-Z.Y. and S.-H.L. contributed equally.

Notes

The authors declare no competing financial interest.

■ ACKNOWLEDGMENTS

This work is financially supported by the National Science and Technology Council (grant nos. NSTC 111-2221-E-005-010 and NSTC 112-2221-E-005-006-MY3), the Innovative Center on Sustainable Negative-Carbon Resources under the Ministry of Education, and the Engineering in Agriculture Biotech Leadership Center of National Chung Hsing University. The Instrument Center and the *i*-Center for Advanced Science and Technology of National Chung Hsing University are gratefully acknowledged for providing the technical support of field-emission scanning electron microscopes.

■ REFERENCES

(1) Zhao, F.; Zhan, F.; Wang, L. Hybrid Topography of Lotus Leaf under Hydrostatic/Hydrodynamic Pressure. *Adv. Mater. Interfaces* **2023**, *10* (4), 220244.

(2) Han, Z. W.; Wang, Z.; Li, B.; Feng, X. M.; Jiao, Z. B.; Zhang, J. Q.; Zhao, J.; Niu, S. C.; Ren, L. Q. Flexible Self-Cleaning Broadband Antireflective Film Inspired by the Transparent Cicada Wings. *ACS Appl. Mater. Interfaces* **2019**, *11* (18), 17019−17027.

(3) Ma, J. Z.; Lu, H. Y.; Li, X. S.; Tian, Y. Interfacial Phenomena of Water Striders on Water Surfaces: A Review From Biology To Biomechanics. *Zool. Res.* **2020**, *41* (3), 231−246.

(4) Avramescu, R. E.; Ghica, M. V.; Dinu-Pîrvu, C.; Prisada, R.; Popa, L. Superhydrophobic Natural and Artificial Surfaces-A Structural Approach. *Materials* **2018**, *11* (5), 866.

(5) Majdoub, H.; Picton, L.; Le Cerf, D.; Roudesli, S. Water Retention Capacity of Polysaccharides from Prickly Pear Nopals of Opuntia Ficus Indica and Opuntia Litoralis: Physical-Chemical Approach. *J. Polym. Environ.* **2010**, *18* (4), 451−458.

(6) Madaeni, S. S.; Falsafi, M.; Ghaemi, N.; Daraei, P. Low-Fouling Biomimetic Membranes Fabricated by Direct Replication of Self-Cleaning Natural Leaf. *Environ. Technol.* **2021**, *42* (23), 3641−3650.

(7) Gao, H. P.; Liu, Y.; Wang, G. Y.; Li, S. Y.; Han, Z. W.; Ren, L. Q. Biomimetic Metal Surfaces Inspired by Lotus and Reed Leaves For Manipulation of Microdroplets or Fluids. *Appl. Surf. Sci.* **2020**, *519*, 146052.

(8) Ge, P.; Wang, S. L.; Zhang, J. H.; Yang, B. Micro-/Nanostructures Meet Anisotropic Wetting: From Preparation Methods to Applications. *Mater. Horiz.* **2020**, *7* (10), 2566−2595.

(9) Peng, Q.; Jia, L.; Ding, Y.; Dang, C.; Yin, L. F.; Yan, X. Influence of Groove Orientation on Dropwise Condensation on Hydrophobic and Hierarchical Superhydrophobic Surfaces with Microgroove Arrays. *Int. Commun. Heat Mass Transfer* **2020**, *112*, 104492.

(10) Liu, C. C.; Ju, J.; Zheng, Y. M.; Jiang, L. Asymmetric Ratchet Effect for Directional Transport of Fog Drops on Static and Dynamic Butterfly Wings. *ACS Nano* **2014**, *8* (2), 1321−1329.

(11) Liu, W. F.; Wang, J. B.; Xu, X. Z.; Zhao, C. Z.; Xu, X. B.; Weiss, P. S. Single-Step Dual-Layer Photolithography for Tunable and Scalable Nanopatterning. *ACS Nano* **2021**, *15* (7), 12180−12188.
(12) He, Q. S.; Zhao, Z. F.; Zhang, H.; Duan, J. J.; Zhang, N.; Cui, K. K.; Zhong, Q. Y.; Yang, C. L. Bioinspired Adhesive Manufactured by Projection Microstereolithography 3D Printing Technology and Its Application. *Adv. Mater. Interfaces* **2023**, *10*, 2202465.
(13) Xu, J. K.; Hou, Y. G.; Lian, Z. X.; Yu, Z. J.; Wang, Z. B.; Yu, H. D. Bio-Inspired Design of Bi/Tridirectionally Anisotropic Sliding Superhydrophobic Titanium Alloy Surfaces. *Nanomaterials* **2020**, *10* (11), 2140.
(14) Zhang, H.; Chen, C. W.; Zhang, H.; Chen, G. P.; Wang, Y. T.; Zhao, Y. J. Janus Medical Sponge Dressings with Anisotropic Wettability for Wound Healing. *Appl. Mater. Today* **2021**, *23*, 101068.
(15) Cai, Z. X.; Chen, F. Z.; Tian, Y. L.; Zhang, D. W.; Lian, Z. X.; Cao, M. Y. Programmable Droplet Transport on Multi-Bioinspired Slippery Surface with Tridirectionally Anisotropic Wettability. *J. Chem. Eng.* **2022**, *449*, 137831.
(16) Narhe, R. D.; Beysens, D. A. Nucleation and Growth on A Superhydrophobic Grooved Surface. *Phys. Rev. Lett.* **2004**, *93* (7), 076103.
(17) Hsu, C. P.; Lin, Y. M.; Chen, P. Y. Hierarchical Structure and Multifunctional Surface Properties of Carnivorous Pitcher Plants *Nepenthes*. *JOM* **2015**, *67* (4), 744−753.
(18) Channing, A.; Wahlberg, K. Distribution And Conservation Status of The Desert Rain Frog *Breviceps Macrops*. *Afr. J. Herpetol.* **2011**, *60* (2), 101−112.
(19) Zhou, S.; Jiang, L.; Dong, Z. C. Bioinspired Surface with Superwettability for Controllable Liquid Dynamics. *Adv. Mater. Interfaces* **2021**, *8* (2), 2000824.
(20) Stoddard, R.; Nithyanandam, K.; Pitchumani, R. Fabrication and Durability Characterization of Superhydrophobic and Lubricant-Infused Surfaces. *J. Colloid Interface Sci.* **2022**, *608*, 662−672.
(21) He, Z. K.; Mu, L. P.; Wang, N.; Su, J.; Wang, Z.; Luo, M. D.; Zhang, C. L.; Li, G. W.; Lan, X. R. Design, Fabrication, and Applications of Bioinspired Slippery Surfaces. *Adv. Colloid Interface Sci.* **2023**, *318*, 102948.
(22) Lv, P.; Zhang, Y. L.; Han, D. D.; Sun, H. B. Directional Droplet Transport on Functional Surfaces with Superwettabilities. *Adv. Mater. Interfaces* **2021**, *8* (12), 2100043.
(23) Ferrín, M.; Márquez, L.; Petersen, H.; Salmon, S.; Ponge, J. F.; Arnedo, M.; Emmett, B.; Beier, C.; Schmidt, I. K.; Tietema, A.; et al. Trait-Mediated Responses to Aridity and Experimental Drought by Springtail Communities Across Europe. *Funct. Ecol.* **2023**, *37* (1), 44−56.
(24) Eckert, M.; Gaigher, R.; Pryke, J. S.; Samways, M. J. Conservation of Complementary Habitat Types and Small-Scale Spatial Heterogeneity Enhance Soil Arthropod Diversity. *J. Environ. Manage.* **2022**, *317*, 115482.
(25) Yun, G. T.; Jung, W. B.; Oh, M. S.; Jang, G. M.; Baek, J.; Kim, N. I.; Im, S. G.; Jung, H. T. Springtail-Inspired Superomniphobic Surface with Extreme Pressure Resistance. *Sci. Adv.* **2018**, *4* (8), 4978.
(26) Hensel, R.; Neinhuis, C.; Werner, C. The Springtail Cuticle as a Blueprint for Omniphobic Surfaces. *Chem. Soc. Rev.* **2016**, *45* (2), 323−341.
(27) Kang, S. M.; Choi, J. S.; An, J. H. Reliable and Robust Fabrication Rules for Springtail-Inspired Superomniphobic Surfaces. *ACS Appl. Mater. Interfaces* **2020**, *12* (18), 21120−21126.
(28) Zhang, Z. G.; Ma, B. H.; Ye, T.; Gao, W.; Pei, G. Y.; Luo, J.; Deng, J. J.; Yuan, W. Z. One-Step Fabrication of Flexible Bioinspired Superomniphobic Surfaces. *ACS Appl. Mater. Interfaces* **2022**, *14* (34), 39665−39672.
(29) Kang, S. M.; Choi, J. S. Selective Liquid Sliding Surfaces with Springtail-Inspired Concave Mushroom-Like Micropillar Arrays. *Small* **2020**, *16* (3), 1904612.
(30) Borah, R.; Ag, K. R.; Minja, A. C.; Verbruggen, S. W. A Review on Self-Assembly of Colloidal Nanoparticles into Clusters, Patterns, and Films: Emerging Synthesis Techniques and Applications. *Small Methods* **2023**, *7* (6), 2201536.
(31) Tufa, L. T.; Jeong, K. J.; Tran, V. T.; Lee, J. Magnetic-Field-Induced Electrochemical Performance of a Porous Magnetoplasmonic Ag@Fe_3O_4 Nanoassembly. *ACS Appl. Mater. Interfaces* **2020**, *12* (5), 6598−6606.
(32) Wang, H.; Chen, W.; Chen, B.; Jiao, Y.; Wang, Y.; Wang, X.; Du, X.; Hu, Y.; Lv, X.; Zeng, Y.; Wang, X.; Qian, L.; Xiong, J. Interfacial Capillary-Force-Driven Self-Assembly of Monolayer Colloidal Crystals for Supersensitive Plasmonic Sensors. *Small* **2020**, *16* (8), 1905480.
(33) Suh, Y.; Pham, Q.; Shao, B. W.; Won, Y. The Control of Colloidal Grain Boundaries through Evaporative Vertical Self-Assembly. *Small* **2019**, *15* (12), 1804523.
(34) Wang, H. Y.; Li, H.; Gu, P.; Huang, C. L.; Chen, S. B.; Hu, C. L.; Lee, E.; Xu, J. P.; Zhu, J. T. Electric, Magnetic, and Shear Field-Directed Assembly of Inorganic Nanoparticles. *Nanoscale* **2023**, *15* (5), 2018−2035.
(35) Conti, Y.; Passarelli, N.; Mendoza-Carreno, J.; Scarabelli, L.; Mihi, A. Colloidal Silver Nanoparticle Plasmonic Arrays for Versatile Lasing Architectures via Template-Assisted Self-Assembly. *Adv. Opt. Mater.* **2023**, *11*, 2300983.
(36) Hsueh, H. Y.; Chen, M. S.; Liaw, C. Y.; Chen, Y. C.; Crosby, A. J. Macroscopic Geometry-Dominated Orientation of Symmetric Microwrinkle Patterns. *ACS Appl. Mater. Interfaces* **2019**, *11* (26), 23741−23749.
(37) Liu, N.; Sun, Q. C.; Yang, Z. S.; Shan, L. N.; Wang, Z. Y.; Li, H. Wrinkled Interfaces: Taking Advantage of Anisotropic Wrinkling to Periodically Pattern Polymer Surfaces. *Adv. Sci.* **2023**, *10* (12), 27.
(38) Lai, Y. F.; Chang, M. Y.; Liou, Y. Y.; Lee, C. C.; Hsueh, H. Y. Morphological Diagram of Dynamic-Interfacial-Release-Induced Surface Instability. *ACS Appl. Mater. Interfaces* **2023**, *15* (32), 38975−38985.
(39) Guvendiren, M.; Yang, S.; Burdick, J. A. Swelling-Induced Surface Patterns in Hydrogels with Gradient Crosslinking Density. *Adv. Funct. Mater.* **2009**, *19* (19), 3038−3045.
(40) Chandra, D.; Crosby, A. J. Self-Wrinkling of UV-Cured Polymer Films. *Adv. Mater.* **2011**, *23* (30), 3441−3445.
(41) da Silva, A. D.; Santos, J. Stöber Method and Its Nuances over the Years. *Adv. Colloid Interface Sci.* **2023**, *314*, 102888.
(42) Hwang, J. H.; Hong, J. S.; Oh, C. W.; Joe, M. J.; Jeong, H. C.; Park, H. G. Soft Imprint Lithography for Liquid Crystal Alignment Using a Wrinkled UVO-Treated PDMS Transferring Method. *J. Mol. Liq.* **2021**, *323*, 115150.
(43) Stafford, C. M.; Harrison, C.; Beers, K. L.; Karim, A.; Amis, E. J.; Vanlandingham, M. R.; Kim, H. C.; Volksen, W.; Miller, R. D.; Simonyi, E. E. A Buckling-Based Metrology for Measuring The Elastic Moduli of Polymeric Thin Films. *Nat. Mater.* **2004**, *3* (8), 545−550.
(44) Sun, T. L.; Song, R. Q.; Balar, N.; Sen, P.; Kline, R. J.; O'Connor, B. T. Impact of Substrate Characteristics on Stretchable Polymer Semiconductor Behavior. *ACS Appl. Mater. Interfaces* **2019**, *11* (3), 3280−3289.
(45) Guo, Y. D.; Zhao, E. Q.; Guo, X. W.; Tang, D. Y. Fabrication of Self-Assembled Hydrophobic Fluorinated Silica Particulate Film. *J. Fluorine Chem.* **2019**, *218*, 27−35.
(46) Matsuyama, K.; Tanaka, S.; Okuyama, T. Hydrophobic Modification of Fibers by Pressure-Induced Phase-Separation Coupled with Ultrasonic Irradiation in High-Pressure Liquid Carbon Dioxide. *Chem. Eng. J.* **2014**, *246*, 106−113.
(47) Gundersen, H.; Leinaas, H. P.; Thaulow, C. Surface Structure and Wetting Characteristics of Collembola Cuticles. *PLoS One* **2014**, *9* (2), No. e86783.
(48) Nickerl, J.; Helbig, R.; Schulz, H. J.; Werner, C.; Neinhuis, C. Diversity and Potential Correlations to The Function of Collembola Cuticle Structures. *Zoomorphology* **2013**, *132* (2), 183−195.
(49) Schmüser, L.; Zhang, W.; Marx, M. T.; Encinas, N.; Vollmer, D.; Gorb, S.; Baio, J. E.; Räder, H. J.; Weidner, T. Role of Surface Chemistry in the Superhydrophobicity of the Springtail *Orchesella cincta* (Insecta:Collembola). *ACS Appl. Mater. Interfaces* **2020**, *12* (10), 12294−12304.

https://doi.org/10.1021/acsanm.4c02117
ACS Appl. Nano Mater. 2024, 7, 14584−14595

(50) Helbig, R.; Nickerl, J.; Neinhuis, C.; Werner, C. Smart Skin Patterns Protect Springtails. *PLoS One* **2011**, *6* (9), No. e25105.
(51) Wawryk, M. M.; Turpin, G. A.; Tabor, R. F. Surface Defects on Wrinkled PDMS Induce Droplet Anisotropy. *Colloids Surf., A* **2022**, *639*, 128317.
(52) Wang, X.; Wang, Z. B.; Heng, L. P.; Jiang, L. Stable Omniphobic Anisotropic Covalently Grafted Slippery Surfaces for Directional Transportation of Drops and Bubbles. *Adv. Funct. Mater.* **2020**, *30* (1), 10.
(53) Hensel, R.; Helbig, R.; Aland, S.; Voigt, A.; Neinhuis, C.; Werner, C. Tunable Nano-Replication to Explore the Omniphobic Characteristics of Springtail Skin. *NPG Asia Mater.* **2013**, *5*, No. e37.
(54) Nickerl, J.; Tsurkan, M.; Hensel, R.; Neinhuis, C.; Werner, C. The Multi-Layered Protective Cuticle of Collembola: a Chemical Analysis. *J. R. Soc., Interface* **2014**, *11* (99), 20140619.
(55) Zhi, J.; Zhang, L.-Z. Durable Superhydrophobic Surface with Highly Antireflective and Self-Cleaning Properties for the Glass Covers of Solar Cells. *Appl. Surf. Sci.* **2018**, *454*, 239−248.
(56) Chi, F.; Liu, D.; Wu, H.; Lei, J. Mechanically Robust and Self-Cleaning Antireflection Coatings from Nanoscale Binding of Hydrophobic Silica Nanoparticles. *Sol. Energy Mater. Sol. Cells* **2019**, *200*, 109939.

https://doi.org/10.1021/acsanm.4c02117
ACS Appl. Nano Mater. 2024, 7, 14584−14595